Mesoporous Silica Nanolayers Infiltrated with Hole-Transporting Molecules for Hybrid Organic Light-Emitting Devices

Jin-Woo Park,[†] Sung Soo Park,[†] Youngkyoo Kim,[‡,*] Il Kim,[†] and Chang-Sik Ha[†,*]

[†]National Research Laboratory of Nano-Information Materials, Department of Polymer Science and Engineering, Pusan National University, Busan 609-735, Republic of Korea, [‡]Organic Nanoelectronics Laboratory, Department of Chemical Engineering, Kyungpook National University, Daegue 702-701, Republic of Korea, and Experimental Solid State Physics Group, Department of Physics, Blackett Laboratory, Imperial College London, Prince Consort Road, London SW7 2BW, United Kingdom

ABSTRACT Organic hole-transporting molecules were infiltrated into inorganic mesochannels *via* hexagonally ordered nanopores that are open at the edge side of mesoporous silica (MS) nanolayers prepared using a block copolymer template. This organic-molecule-infiltrated MS nanolayer was used as a hole injection/transport layer for hybrid organic light-emitting devices (HOLED) for improving the device stability. The result showed that the efficiency of HOLED is within reach of that of conventional devices, promising further improvement by the thickness control.

KEYWORDS: mesoporous silica · infiltrated organic light-emitting device · hybrid nanolayer · hole injection layer · hole transporting layer

The first mesoporous molecular sieves based on silica were reported in 1992, which were called M41S materials of which pores featured hexagonal, cubic, and lamellar structures.[1−3] The nanopores (2∼50 nm) of mesoporous inorganic materials are typically made by eliminating the ordered soft nanodomains (organic surfactants) surrounded by a rigid inorganic (*e.g.*, silica) frame *via* calcinations and/or ion exchange processes.[4] In particular, the size and geometry of the nanopores can be easily controlled by varying sorts of organic surfactants, pH of precursor solutions, hydrothermal treatment conditions, *etc.*

These surfactant-templated mesoporous inorganic structures were used as a host nanostructure to bind guest molecules in composites[5] in applications for high-surface-area catalysis,[6] molecular separation,[7] pH-sensors by incorporating pH-sensitive dyes,[8] gas sensors,[9] and insulating dielectric layers.[10] In addition, their thin films were applied for the inclusion of organic materials because the mesochannels formed in the thin film of mesoporous materials could trap gaseous or liquid organic materials (for example, a template-free mesoporous film based humidity sensor that exhibits an electrical current variation upon uptaking moistures).[11] Wu *et al.* reported the oriented polymer/silica composites synthesized by incorporating poly[2-methoxy-5(2′-ethyl-hexyloxy)-1,4-phenylene vinylene] (MEH-PPV) into the pores of the aligned and hexagonally ordered mesoporous silica.[12] Very recently, Molenkamp *et al.* reported the highly aligned mesoporous silica films filled with MEH-PPV as a promising new class of host/guest structure in which the polymer chains exhibited a high degree of dipole alignment due to their confinement within the silica frames.[13] However, these mesoporous materials have not yet been applied for organic light-emitting devices (OLED), even though we briefly reported a hybrid OLED (HOLED) with amorphous silica-dye composite films prepared by in situ sol−gel reaction.[14]

In this work, we have attempted to make highly ordered mesoporous silica (MS) nanolayers (nanofilms), of which mesochannels are infiltrated with hole-transporting molecules, *N*,*N*′-diphenyl-*N*,*N*′-bis(3-methylphenyl)-1,1-biphenyl-4,4′-diamine) (TPD), as a stable hole injection/transport layer (HITL). The idea here is that the thermally and mechanically (geometrically) strong MS frames could help overcome the weakness of unstable but relatively cheap organic semiconducting materials such as the TPD molecule that was already confirmed as the unreliable material for thin films.[15] If this idea works, its application can be extended to improve the device reliability of OLEDs which still lags behind the requirements for consumer display device applications despite ongoing remarkable advances [Note that OLED displays in market show the device lifetime less than 150 h at 90 °C (<10000 h at room temperature)].[16−18]

*Address correspondence to csha@pusan.ac.kr, ykimm@knu.ac.kr.

Received for review October 22, 2007 and accepted April 19, 2008.

Published online May 17, 2008.
10.1021/nn7003124 CCC: $40.75

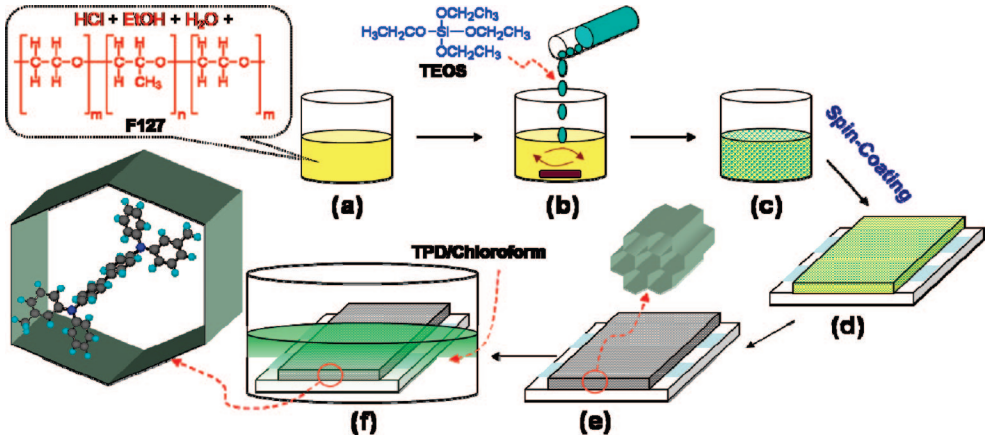

Figure 1. Schematic illustration for the preparation of TIMS nanolayers: (a) starting solution containing organic template (F127) and catalysts, (b) dropping TEOS into the solution in container a, (c) resulting precursor solution, (d) precursor nanolayer spun onto ITO glass, (e) MS nanolayer (see hexagonal nanopores) obtained by calcinations from structure d, and (f) infiltration of TPD molecules into the nanopores of MS nanolayer to make corresponding TIMS nanolayer.

RESULTS AND DISCUSSION

Preparation and Resulting Nanomorphology. Optically transparent hexagonally ordered MS nanolayers were synthesized using the modified procedure (see Figure 1 and Methods section) from the reported method.[19,20] The present modified procedure makes a hexagonal nanopore structure because corresponding precursor solution is not heated but just stirred at room temperature for a longer time (~5 h) before spin-coating to allow slow and organized growth of sol−gel intermediates, whereas a cubic structure is made by the conventional procedure in refs 19 and 20 which heats the precursor solution at 50~80 °C resulting in a quick growth of sol−gel intermediates.

Figure 2 shows the nanomorphology of MS or TPD-infiltrated MS (TIMS) nanolayers. The SEM image shows a well-controlled MS nanolayer exhibiting a nanoporous structure in its edge region despite the deformed shape arisen upon breaking the sample for measurement (see Figure 2a). Here the TEM images show that these nanopores in the edge of the nanolayer are highly ordered featuring a hexagonal nanostructure (see X1 and X2 in Figure 2d), while the surface of this nanolayer is made with the extremely organized nanostripes or nanotubes (see Y1 in Figure 2d and Figure 2e). This nanotubular surface structure is confirmed from the AFM images (see Y2 and Y3 in Figure 2b,c). Therefore, the present MS nanolayers have a mesochannel structure of which nanopores are open in the edge side but closed on the surface direction. However, considering the AFM images, the mesochannels (mesotubes) are not linearly shaped but are mixed with highly ordered regions (see Y2 and Y3 in Figure 2b,c; Y1 in Figure 2d; Figure 2e) and disordered interfacial domains (see Z1~Z4 in Figure 2b,c). In particular, the very small nanospots (see P1 in Figure 2c) are considered as a defect (*e.g.*, amorphous silica) made during the precursor film preparation and/or calcination processes. Hence, during the immersion process of the MS nanolayers in the TPD/chloroform solution the TPD molecules could be infiltrated through the nanopores at the layer edge of which the size is estimated to be 5~8 nm with the TEM image (see Figure 2d,f), resulting in the TIMS nanolayer substrates for HOLEDs (see Figure 2g for the size comparison between the TPD molecule and the nanopore). We note that the TEM and AFM images were almost similar between the pristine MS and TIMS nanolayers. In addition, we note that the present morphology examinations do not show any serious

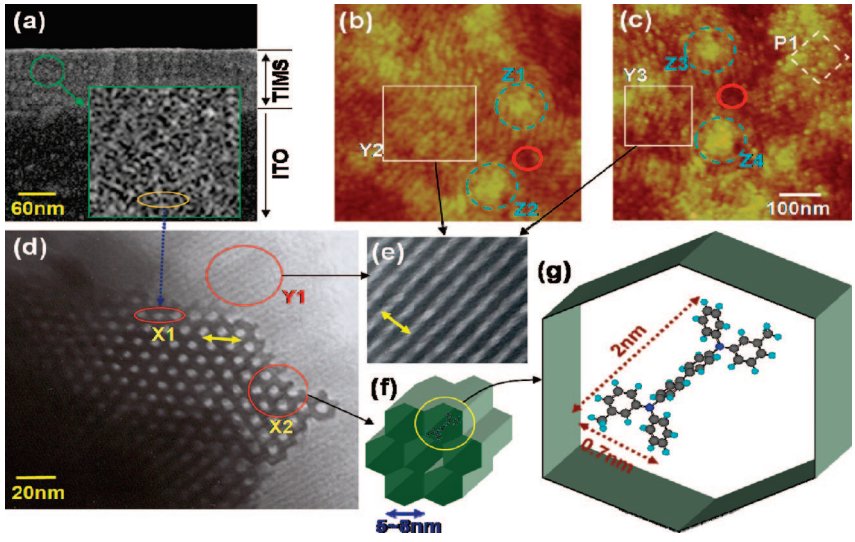

Figure 2. Nanomorphology of MS or TIMS nanolayers: (a) SEM image for the cross-sectional area of nanolayer [see the nanopores in the enlarged part and more clear view in panel d]; (b,c) AFM images exhibiting two types (b and c) of surface nanomorphology mixed in actual nanolayers which feature less-ordered domains (Z1~Z4), nanospots (P1), and interfaces between highly ordered domains (see circles in orange color); (d) TEM image of tilted nanolayer to show both edge (dotted region) and surface (striped region) sides [note that the exact size of nanopores can be measured from the closest front side ones (X2) owing to the tilted image]; (e) TEM image of the surface side of the nanolayer [see (d) Y1, (b) Y2, and (c) Y3]; (f) schematic illustration for the dotted region (see X2) in the TEM image d; and (g) enlarged drawing from one nanopore of structure f [note that the size of silica frame is not drawn to the actual dimensions owing to the limited space in this figure].

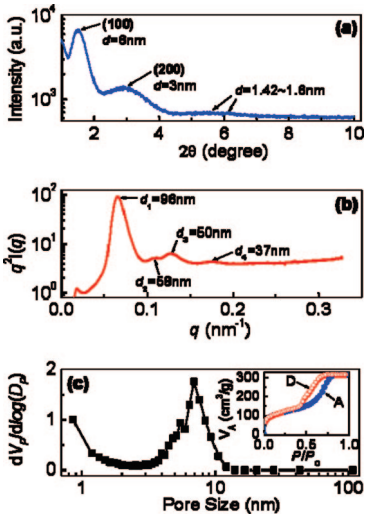

Figure 3. Characteristics of MS nanolayers: (a) WAXD pattern as a function of diffraction angle (2θ), (b) Lorentz-corrected SAXS profile as a function of scattering vector (q) (ref 31), (c) pore size distribution by BHJ method [V_P and D_P denote a pore volume and a pore diameter, respectively. Inset shows nitrogen adsorption (A)−desorption (D) isotherms showing adsorbed volume (V_A) as a function of relative pressure].

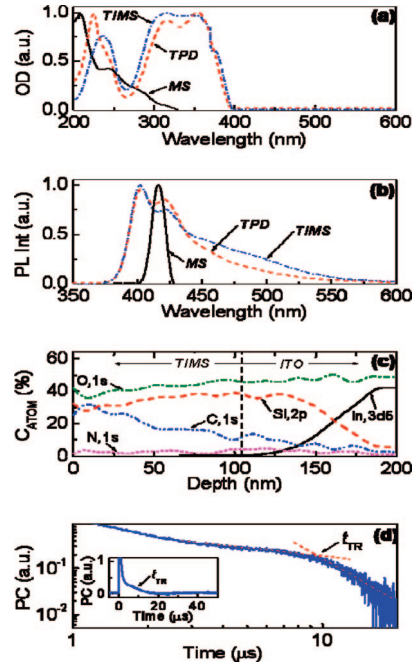

Figure 4. Characteristics of TIMS nanolayers: (a) normalized optical density (OD) spectra (TPD and MS samples were measured for comparison); (b) normalized photoluminescence (PL) spectra (TPD and MS samples were measured for comparison. The excitation wavelengths were 208, 316, and 314 nm for MS, TPD, and TIMS samples, respectively); (c) atom concentration (C_{ATOM}) in the TIMS nanolayer (thickness = 110 nm) as a function of thickness, and (d) logarithmic photocurrent (PC) transient of TIMS nanolayer (thickness = 400 nm) as a function of time (see linear scale in inset; t_{TR} represents the inflection point).

cracks that could make possible vertical pathways for charge transport and/or leakage.

Characterization of Nanopores. As shown in Figure 3a, the WAXD pattern exhibits the obvious (100) diffraction peak at 2θ=1.49° leading to the d-spacing of ~6 nm that is well positioned in the middle of the pore size (5~8 nm) measured using the TEM in Figure 2. In particular, the second order (200) peak 2θ = 2.93° confirms how regularly the nanopores are made inside the MS nanolayer, even though the third-order peak is hidden with the weak and broad reflection peaks at around 2θ = 4.5°~7° which are attributed to amorphous parts as observed in the AFM images (Z1~Z4 in Figure 2b,c). These amorphous parts can be explained by the SAXS profile that shows a multidomain nanostructure which varies in size from 37 to 96 nm (see d_1~d_4 in Figure 3b). This indicates the existence of polycrystalline (or partial amorphous) structures in the nanolayer, which is supported from the AFM images in Figure 2.

As shown in Figure 3c, the pore size (average diameter) of MS nanolayers were calculated as ~7 nm using the BJH method (see Methods section),[21,22] which is very similar to those values measured with TEM (5~8 nm) and WAXD (6 nm). The specific surface area was determined to be 1693 m^2/g (1.693 × 10^{21} nm^2/g) according to the BET method,[21] while the calculated pore volume was 0.7 cm^3/g from the adsorbed volume as a function of pressure using the BJH method.[19,20,22] Here we note that the present MS nanolayer shows the largest surface area among those reported previously,[19,20] which might be attributed to the correlation of lower pore volume and smaller diameter. This result indicates that the pore volume of the TIMS nanolayer per each pixel in OLEDs is ~3 × 10^{14} nm^3, considering its whole volume per pixel (4.4 × 10^{14} nm^3). Therefore, assuming the volume (~1 nm^3) of a single TPD molecule (see its dimension in Figure 2g), the ideal number of TPD molecules infiltrated into the MS nanolayer per each pixel is approximately ~3 × 10^{14}.

Evidence of Infiltration Leading to TIMS Nanolayer. As shown in Figure 4a,b, optical measurements show clear evidence that the TPD molecules were infiltrated into the MS mesochannels. The optical density spectrum of the TIMS nanolayer does excellently follow that of the pristine TPD film even though its absorption peak at the shorter wavelength range (200~250 nm) was shifted toward a lower energy part (see Figure 4a). Similarly, the photoluminescence (PL) spectrum of the TIMS nanolayer resembles that of the pristine TPD film (see Figure 4b). Here the increased intensity of the TIMS nanolayer at the wavelength between 430 and 570 nm is considered as an interaction between the lone pair electrons in the nitrogen atoms of TPD molecules and the unsaturated hydroxyl groups of inner silica walls, which would also be the reason for the lower PL intensity at 450 nm peak for the TIMS nanolayer. We note that the MS nanolayer showed only weak PL spectrum which is obviously different from those of TPD film or TIMS nanolayer.

However, the XPS investigation shows that the relative composition of TPD decreases as the pore position is closer to the substrate (see the C1s peak trend in Figure 4c): We note that the N1s (N−C bonding) peak is not so reliable because of very low concentration even though it is very different in energy from that of N_2 gas that could be possibly adsorbed in the pores because all processes were performed inside a nitrogen-filled glovebox. Therefore, the population of infiltrated TPD molecules might be far lower than the ideal number (*i.e.*, $\ll 3 \times 10^{14}$). As shown in Figure 4d, the photocurrent transient by TOF measurement[23,24] exhibits an inflection point at around $t_{TR} = 9.8$ μs, which results in the hole mobility [$\mu = d^2/(E \times t_{TR})$] of 1.02×10^{-10} cm^2 V^{-1} s^{-1} at an electric field (E) of 2×10^6 V cm^{-1}. This mobility is very lower than that (5.7×10^{-5} cm^2 V^{-1} s^{-1} at $E = 5 \times 10^5$ V cm^{-1}) reported by Morais *et al.*[25] for the TPD modified silica precursor sol−gel material. This low mobility of the TIMS film can be attributed to the "effective" charge blocking of silica walls (about 11 walls with 3∼5 nm thick for each pore in the thickness direction of the 110 nm thick nanolayer), because a limited charge transport is expected for the 3∼5 nm thick inorganic layers such as SiO_2 or LiF depending on their packing densities (this will be discussed again in Figure 5).[26,27] In addition, the low concentration of TPD molecules, particularly in the vicinity of ITO anode as confirmed with the XPS measurement, might be responsible for the low hole mobility as observed previously by diluting TPD molecules in a polycarbonate matrix.[28]

Device Characteristics. As shown in the inset to Figure 5 (top panel), almost no current flow across the electrode was detected for the control devices with the MS nanolayer (and/or the inserted TPD layer in between MS and Alq3 layers). This proves that the MS nanolayer (without TPD molecules) is absolutely an insulating layer, whereas the TIMS nanonalyer (infiltrated with TPD molecules) is a semiconducting layer. The J-V-L characteristics of OLEDs with the TIMS nanolayer exhibit a thickness-dependent trend (see Figure 5 top and middle panels): The best device performance was achieved at the Alq3 thickness of 70 nm (see the photograph of actually operated HOLED in the middle panel of Figure 5), whereas the thinner or thicker Alq3 layer resulted in the poorer performance. Although this thickness-dependent trend is also observed for the TPD devices, its influence is more pronounced for the TIMS devices because the required electric field (or voltage) across the electrodes at the same current density (or luminance) is much higher for the TIMS devices than the TPD devices. This strongly indicates that the present TIMS nanolayer controls the hole current as expected from the measured hole mobility for the thick TIMS film in Figure 4d. In addition, the diode characteristics (*i.e.*, diode ideality or upturn behavior) in J-V curves[29] are poorer for the TIMS devices than the TPD devices irrespective of the active layer thickness (see Figure 5 top panel). This is also attributed to the very low mobility of TIMS films having the relatively thick (3∼5 nm) silica walls (see Figure 4d) which is expected to be more electric field-dependent than the pristine TPD films.

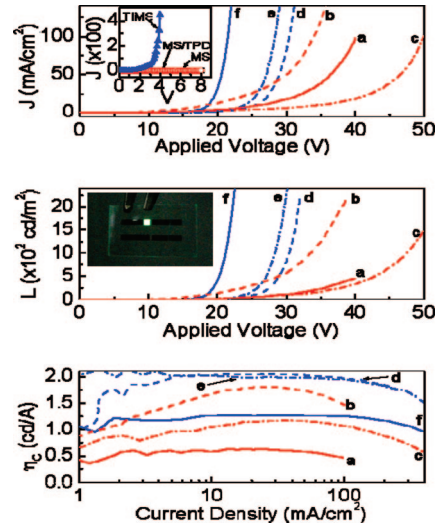

Figure 5. *J*−*V* (top panel), *L*−*V* (middle panel), and current efficiency (η_C)−*J* (bottom panel) characteristics of HOLEDs with TIMS nanolayers (110 nm) and Alq3 ((a) 50, (b) 70, (c) 110 nm), OLEDs with TPD layers (110 nm) and Alq3 ((d) 70, (e) 110 nm), and (f) OLED with TPD layer (50 nm) and Alq3 (50 nm). Inset to the top panel shows *J*−*V* characteristics of devices of which active layers in between ITO and Al electrodes are TIMS (110 nm)/Alq3 (70 nm), MS (110 nm)/Alq3 (70 nm), and MS (110 nm)/TPD (50 nm)/Alq3 (70 nm). The photograph in the middle panel shows the image of the operated HOLED (ITO/TIMS (110 nm)/Alq3 (70 nm)/Al) at 15 V.

Despite this pronounced hole confining effect of the TIMS nanolayer, the current efficiency of the TIMS devices (except "b" device) was generally lower than that of the TPD devices (see Figure 5 bottom panel). However, the "b" device with the 70 nm thick TIMS nanolayer showed very close efficiency to the TPD devices at the same Alq3 thickness. This result implies a very promising future for the TIMS nanolayer as the HITL in OLEDs, and proposes further control of the TIMS nanolayer thickness in order to reduce the turn-on voltage for enhancing the maximum luminance, seen from the TPD device with the reduced TPD thickness (see "f" in Figure 5): Here no significant device degradation is expected for the TIMS device by reducing the TIMS thickness due to the stabilizing of TPD molecules by durable MS walls, whereas the catastrophic deterioration is observed frequently for the thinner TPD devices.[30] Finally, we noticed that the Commission Internationale de l'Eclairage (CIE) chromaticity coordinate (x, y) was almost not changed for the HOLED with the 70 nm thick TIMS nanolayer, whereas it was changed from (0.31, 0.56) to (0.32, 0.55) upon increasing the applied voltage up to 32 V for the TPD device.

CONCLUSIONS

The MS nanolayers were successfully prepared to have mesochannels with hexagonally ordered nanopores in a size of 5~8 nm, of which the mouth was open at the edge side so that the TPD molecules could be infiltrated into the mesochannels. However, the surface morphology showed that the mesochannels are nonlinearly oriented along with the substrate plane, resulting in multidomain polycrystals. The concentration of infiltrated TPD molecules was lower at the ITO electrode side than at the surface side, which might contribute to the very low hole mobility. The current efficiency of HOLED with the TIMS nanolayer was within reach of that of OLED with the pristine TPD layer at the same thickness, promising a further improvement in device performance and reliability as well, when it comes to the well-defined and thermally/mechanically durable silica nanostructures. Finally, we propose following two methods to improve the present device performance: (1) The present TIMS nanolayer has insufficient incorporation of TPD molecules into the pores, leading to low hole mobility. This could be improved by modifying the silica wall with alkyl groups *via* employing organosilica precursors since nonpolar TPD molecules can easily path through the modified nonpolar walls. (2) The device performance could be also improved by optimizing the silica wall thickness as well as the pore size to achieve reduced electrical resistance and improved degree of incorporation into pores.

METHODS

Materials and Preparation of MS and TIMS Nanolayers. The first step in the modified procedure is to prepare the mixture solution consisting of deionized water (H_2O) (12 mol), hydrochloric acid solution (35% HCl, Junsei Chemical) (3.0×10^{-2} mol), anhydrous ethanol (EtOH, Aldrich, 99.9%) (60 mol), and poly(ethyleneoxide)-*block*-poly(propylene oxide)-*block*-poly(ethylene oxide) ($EO_{106}PO_{70}EO_{106}$, F127, Aldrich) (1.0×10^{-2} mol) as an organic templating surfactant, which was vigorously stirred at room temperature for 2 h (see Figure 1a). Next, tetraethoxysilane (TEOS, Aldrich, 98%) (1 mol) was slowly added to the previous mixture solution with vigorous stirring at room temperature for 2 h (see Figure 1b), resulting in the precursor sol solution for the target MS nanolayers (see Figure 1c).

Prior to spin-coating, indium−tin oxide (ITO) coated glass substrates were patterned in a strip size of 2 mm × 20 mm, followed by wet and dry cleaning in the same way as described in refs 15 and 16. Then the precursor sol solution was spin-coated onto the cleaned ITO glass substrate at 6000 rpm for 50 s (1000 rpm for 20 s to make a 400 nm thick film for the hole mobility measurement) and the spun films (nanolayers) were subject to softbaking in a drying oven (air) at 80 °C for 2 h (see Figure 1d). The dried MS precursor nanolayers that are coated on the ITO glass substrate were calcined in air flow at 450 °C for 4 h at a ramp rate of 1 °C/min to remove the organic templating surfactant (see Figure 1e). After the calcination process, all samples were stored immediately in a nitrogen-filled glovebox before use for preventing any possible absorption of moisture. Inside the nitrogen-filled glovebox the prepared MS nanolayers were immersed in the chloroform solution containing 3 wt % TPD molecules (Tokyo Kansei Kogyo Co.) and remained for 8 h to give sufficient time for the inclusion of TPD molecules into the mesochannels (nanopores) of MS nanolayers (see Figure 1f). Finally, after taking out the substrates, the possibly adhered TPD molecules on the surface of the nanolayers were whisked off by spinning them at 5000 rpm for 5 s under a nitrogen gas shower. The thickness of resulting TPD-infiltrated mesoporous silica (TIMS) nanolayers was 110 nm.

Device Fabrication. To make OLEDs, tris(8-hydroxyquinolinato)-aluminum (Alq3, Tokyo Kansei Kogyo Co.) layers (thickness = 50, 70, and 100 nm) as an emission layer were thermally deposited on top of the TIMS nanolayers in a vacuum of 5×10^{-6} Torr, followed by depositing the aluminum (Al) electrode as a cathode, defining the active pixel area of 0.04 cm^2. For making comparison (control) OLEDs the pristine TPD layer with the same thickness was used instead of the TIMS layer, while the thin TPD device with the 50 nm thick TPD layer was made to check the reduction of turn-on voltage by decreasing the layer thickness. To prove the clear role of TIMS nanolayer as the HITL, two kinds of OLED were additionally fabricated: ITO/MS (110 nm)/Alq3 (70 nm)/Al and ITO/MS (110 nm)/TPD (50 nm)/Alq3 (70 nm)/Al. To make the devices for hole mobility measurements, the Al electrode was directly deposited on the differently made thick TIMS films (thickness = 400 nm). The thickness of all films was cross-checked using a surface profiler (α-step IQ, KLA, Tencor).

Nanomorphology and Nanostructure Investigation. The nanomorphology of pristine MS and TIMS nanolayers was investigated using transmission electron microscopy (TEM, 200 kV, JEOL JEM-2010), scanning electron microscopy (SEM, 10 kV, JEOL KEVEX Sigma), and atomic force microscopy (AFM, Nanoscope IIIa, Digital Instrument). The fine nanostructure of the MS films were measured using a reflection mode wide-angle X-ray diffraction (WAXD, Rigaku Multiplex instrument) with Cu Kα (λ=0.15406 nm) radiation operated at 50 KV and 30 mA (1.5 KW). The long-range (larger) nanostructure of MS nanolayers was measured with small-angle X-ray scattering (SAXS) using a synchrotron radiation source [Co−Kα (λ = 1.608 Å); energy range = 4~16 keV; energy resolution ($\Delta E/E$) = 5×10^{-4}; photon flux = 10^{10}~10^{11} ph./s; beam size = <1 mm; Pohang Accelerator Laboratory, Korea] over the scan range of 0.0027 $nm^{-1} < q$ (scattering vector) < 2.7508 nm^{-1}.

Optical, Pore Size, and Composition Characterization. The optical density spectra of samples were measured using a UV−visible spectrometer (Hitachi U-2010) while the photoluminescence spectra were measured using a fluorescence spectrophotometer (Hitachi F-4500). The pore size distribution of MS nanolayers was calculated using the Barrett−Joyner−Halenda (BJH) method[21,22] after measuring the adsorption−desorption isotherms of nitrogen at −196 °C using an adsorption analyzer (Qunatachrome Nova 4000e): All samples were outgassed at 150 °C for 12 h under vacuum (<5×10^{-6} Torr) in the degassing port. The atomic concentration in the thickness direction of TIMS nanolayers was measured by depth-profiling using a monochromatized X-ray photoelectron spectrometer (XPS, ESCALAB 250 XPS spectrometer, VG Scientifics) equipped with the X-ray radiation source of Alkα (1486 eV).

Charge Mobility and Device Measurements. The hole mobility of thick TIMS films (thickness = 400 nm) was measured using a specialized time-of-flight (TOF) measurement system equipped with a digital storage oscilloscope (WaveRunner 6051A; LeCroy) and a nitrogen-pumped dye laser (λ =337 nm; spectral bandwidth = 0.1 nm; pulse width = <4 ns; Spectra-Physics Co.) by controlling 50 Ω resistor. The current density−voltage−luminance ($J-V-L$) characteristics and electroluminescence (EL) spectra were measured using a custom measurement system equipped with an electrometer (SMU 236, Keithley), photomultiplier tube (PMT) (Hamamatsu Photonics, Co.), and a candela meter (PR 650, Photo Research Inc.).

Acknowledgment. The work was supported by the Korea Science and Engineering Foundation (KOSEF) through the National Research Laboratory Program funded by the Ministry of Science and Technology (MOST) (No. M10300000369-06J0000-36910), the SRC/ERC of MOST/KOSEF program (Grant No. R11-2000-070-080020), and the Brain Korea 21 Project.

REFERENCES AND NOTES

1. Kresge, C. T.; Leonowicz, M. E.; Roth, W. J.; Vartuli, J. C.; Beck, J. S. Ordered Mesoporous Molecular Sieves Synthesized by a Liquid-Crystal Template Mechanism. *Nature* **1992**, *359*, 710–712.
2. Beck, J. S.; Rartuli, J. C.; Roth, W. J.; Leonowicz, M. E.; Kresge, C. T.; Schmitt, K. D.; Chu, C. T.; Olson, D. H.; Sheppard, E. W.; McCullen, S. B.; Higgins, J. B.; Schenker, J. L. A New Family of Mesoporous Molecular Sieves Prepared with Liquid Crystal Templates. *J. Am. Chem. Soc.* **1992**, *114*, 10834–10843.
3. Kresge, C. T.; Leonowicz, M. E.; Roth, W. J.; Vartuli, J. C. Ordered Mesoporous Molecular Sieves Synthesized by a Liquid-Crystal Template Mechanism *U.S. Patent* 5,098,684, 1992.
4. Hou, Q; Margolese, D. I.; Stucky, G. D. Surfactant Control of Phases in the Synthesis of Mesoporous Silica-Based Materials. *Chem. Mater.* **1996**, *8*, 1147–1160.
5. Wei, Y.; Yeh, J. M.; Jin, D.; Jia, X.; Wang, J. Composites of Electronically Conductive Polyaniline with Polyacrylate-Silica Hybrid Sol-Gel Materials. *Chem. Mater.* **1995**, *7*, 969–974.
6. Yang, H.; Coombs, N.; Sokolov, I.; Ozin, G. A. Registered Growth of Mesoporous Silica Films on Graphite. *J. Mater. Chem.* **1997**, *7*, 1285–1290.
7. Park, D. H.; Nishiyama, N.; Egashira, Y.; Ueyama, K. Enhancement of Hydrothermal Stability and Hydrophobicity of a Silica MCM-48 Membrane by Silylation. *Ind. Eng. Chem. Res.* **2001**, *40*, 6105–6110.
8. Wirnsberger, G.; Scott, B. J.; Stucky, G. D. pH Sensing with Mesoporous Thin Films. *Chem. Commun.* **2001**, 119–120.
9. Cabot, A.; Arbiol, J.; Cornet, A.; Morante, J. R.; Chen, F.; Liu, M. Mesoporous Catalytic Filters for Semiconductor Gas Sensors. *Thin Solid Films* **2003**, *436*, 64–69.
10. Yang, C.; Cho, A.; Pan, R.; Tsai, T.; Chao, K. Spin-on Mesoporous Silica Films with Ultralow Dielectric Constants, Ordered Pore Structures, and Hydrophobic Surfaces. *Adv. Mater.* **2001**, *13*, 1099–1102.
11. Bearzotti, A.; Bertolo, J. M.; Innocenzi, P.; Falcaro, P.; Traversa, E. Humidity Sensors Based on Mesoporous Silica Thin Films Synthesized by Block Copolymers. *J. Eur. Ceram. Soc.* **2004**, *24*, 1969–1972.
12. Wu, J.; Gross, A. F.; Tolbert, H. Host-Guest Chemistry Using an Oriented Mesoporous Host: Alignment and Isolation of a Semiconducting Polymer in the Nanopores of an Ordered Silica Matrix. *J. Phys. Chem.* **1999**, *103*, 2374–2384.
13. Molenkamp, W. C.; Watanabe, M.; Miyata, H.; Tolbert, S. H. Highly Polarized Luminescence from Optical Quality Films of a Semiconducting Polymer Aligned within Oriented Mesoporous Silica. *J. Am. Chem. Soc.* **2004**, *126*, 4476–4477.
14. Keum, J.; Kang, E.; Kim, Y.; Cho, W. J.; Ha, C. S. Organic/Inorganic Hybrid Electroluminescent Devices Prepared *via* Sol-Gel Process. *Mol. Cryst. Liq. Cryst.* **1998**, *316*, 297–300.
15. Kim, Y.; Keum, J.; Lee, J. G.; Lim, H.; Ha, C. S. Non-linear Charge Conduction and Emission Behavior of OELD Fabricated with Alq_3 and TPD-Doped Soluble Polyimide. *Adv. Mater. Opt. Electron.* **2000**, *10*, 273–300.
16. Kim, Y.; Choi, D.; Lim, H.; Ha, C. S. Accelerated Pre-oxidation Method for Healing Progressive Electrical Short in Organic Light-Emitting Devices. *Appl. Phys. Lett.* **2003**, *82*, 2200–2202.
17. Pfeiffer, M.; Forrest, S. R.; Zhou, X.; Leo, K. A Low Drive Voltage, Transparent, Metal-free n-i-p Electrophosphorescent Light Emitting Diode. *Org. Electron.* **2003**, *4*, 21–26.
18. Kim, Y.; Oh, E.; Choi, D.; Lim, H.; Ha, C. S. Efficient Blue Organic Light-Emitting Devices with Charge Carrier Confining Nanostructure Formed by Wide Band Gap Molecule Doping. *Nanotechnology* **2004**, *15*, 149–153.
19. Zhao, D.; Yang, P.; Melosh, N.; Feng, J.; Chmelka, B. F.; Stucky, G. D. Continuous Mesoporous Silica Films with Highly Ordered Large Pore Structures. *Adv. Mater.* **1998**, *10*, 1380–1385.
20. Zhang, F.; Yan, Y.; Yang, H.; Meng, Y.; Yu, C.; Tu, B.; Zhao, D. Understanding Effect of Wall Structure on the Hydrothermal Stability of Mesostructured Silica SBA-15. *J. Phys. Chem. B* **2005**, *109*, 8723–8732.
21. Brunaurr, S.; Emmett, P. H.; Teller, E. Adsorption of Gases in Multimolecular Layers. *J. Am. Chem. Soc.* **1938**, *60*, 309–319.
22. Barrettzp, E. P.; Joyner, L. G.; Halenda, P. P. The Determination of Pore Volume and Area Distributions in Porous Substances. I. Computations from Nitrogen Isotherms. *J. Am. Chem. Soc.* **1951**, *73*, 373–380.
23. Meier, H. *Organic Semiconductors;* Verlag Chemie: Weinheim, Germany, 1974; p 101.
24. Kim, Y.; Bae, K. H.; Jeong, Y. Y.; Choi, D. K.; Ha, C. S. An Electronically Active Molecularly Doped Polyimide Hole Injection Layer for an Efficient Hybrid Organic Light-Emitting Device. *Chem. Mater.* **2004**, *16*, 5051–5057.
25. Morais, T. D.; Chaput, F.; Boilot, J. P.; Lahlil, K.; Darraiq, B.; Levy, Y. Hole Mobilities in Sol-Gel Materials. *Adv. Mater. Opt. Electron.* **2000**, *10*, 69–79.
26. Deng, Z. B.; Ding, X. M.; Lee, S. T.; Gambling, W. A. Enhanced Brightness and Efficiency in Organic Electroluminescent Devices Using SiO_2 Buffer Layers. *Appl. Phys. Lett.* **1999**, *74*, 2227–2229.
27. Hung, L.S.; Chen, C. H. Recent Progress of Molecular Organic Electroluminescent Materials and Devices. *Mater. Sci. Eng., R* **2002**, *39*, 143–222.
28. Stolka, M.; Yanus, J. F.; Pai, D. M. Hole Transport in Solid Solutions of a Diamine in Polycarbonate. *J. Phys. Chem.* **1984**, *88*, 4707–4714.
29. Sze, S. M. *Physics of Semiconductor Devices,* 2nd ed.; John Wiley & Son: New York, 1981; pp 63−122..
30. Kim, Y.; Lee, J. G.; Han, K.; Hwang, H.K.; Choi, D. K.; Jung, Y. Y.; Keum, J. H.; Kim, S.; Park, S. S.; Im, W. B. Hole-Transporting Polyimide for Organic Electroluminescent Display. *Thin Solid Films* **2000**, *363*, 263–267.
31. Chuang, W. T.; Jeng, U. S.; Sheu, H. S.; Hong, P. D. Competition between Phase Separation and Crytallization in a PCL/PEG Polymer Blend Captured by Synchronized SAXS, WAXS, and DSC. *Macromol. Res.* **2006**, *14* (3), 257–262.